Magazine of Civil Engineering

ISSN 2712-8172

journal homepage: http://engstroy.spbstu.ru/

Research article

UDC 624

DOI: 10.34910/MCE.116.9

An improved lateral restrained local fuse used in concentric braces

A. Kachooee

Amin University, Tehran, Iran

✉ *ali.kachooee@semnan.ac.ir*

Keywords: local fuse, concentric bracing, ductility capacity, energy absorption capacity, load bearing capacity, steel structures

Abstract. The present paper continues a series of the authors' studies on improving conventional concentrically braced frames (CBFs). In previous works, the authors equipped a CBF with a restrained local fuse to improve its behavior, thus introducing local fuse–auxiliary element concentric braces (LF-AECBs). The mechanism of LF-AECBs with a restricted fuse in the length increased the ductility and energy dissipation capacity of the bracing system by limiting the overall buckling locally to the compressive zone. However, further numerical studies suggested that due to early buckling, now local, the restrained local fuse could not be exploited until the failure. Therefore, this study introduces an improved local fuse–auxiliary element concentric brace (ILF-AECB) to fix the issue. Numerical studies are also done to determine the optimal shape of ILF-AECBs in order to obtain maximum energy dissipation capacity and ductility under cyclic loading. In this article, the results of experimental and numerical studies show that ILF-AECBs with a new formulation delaying the fuse buckling completely succeed in using the full capacity of the local fuse for energy dissipation and ductility. Moreover, the analytical study shows that the frame equipped with ILF-AECB offered much better performance in terms of energy dissipation and reduction of the input demand to the structural elements compared to the similar CBFs.

Citation: Kachooee, A. An improved lateral restrained local fuse used in concentric braces. Magazine of Civil Engineering. 2022. 116(8). Article no. 11609. DOI: 10.34910/MCE.116.9

1. Introduction

An off-center bracing system was introduced by Moghaddam and Estekanchi [1]. This structural system was invented for improving concentrically braced frame (CBF) behavior [2]. As shown in Fig. 1, it basically consists of the non-straight tension strut AOC with an eccentricity designated as *e*. The midpoint is connected to the corner by the third member. Once the load is applied, all these three members are stretched, therefore, act in tension. In the recent decade, some research has been conducted on this structural system [3–6]. In [6], some numerical studies have been performed using the ANSYS software on a frame with off-center bracing system with optimum eccentricity and circular element created, called the OBS_C_O model. The obtained results revealed that it would be useful to use a circular dissipater for increasing the ductility of off-center bracing system.

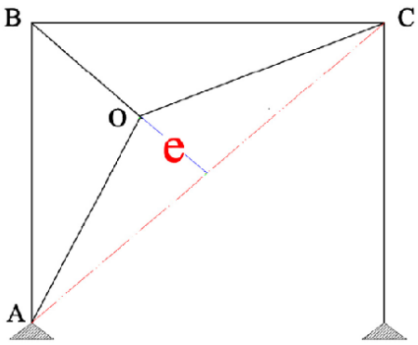

Figure 1. Off-center bracing system.

A cast modular ductile bracing system (CMDB) was introduced as an alternative for the special CBF structures [7, 8]. As shown in Fig. 2, these structural systems are made of a cast component in the middle and ends of the braces. A cruciform cross-section is utilized for CMDB because this section increases energy dissipation capacity and low cycle fatigue life; in turn, they cause reduced brace failure probability. A system similar to the above one was proposed by Seker et al. to replace the conventional concentric braces [9]. The system uses a three-part steel brace and the idea behind it is to develop an elastic buckling extension of a multi-part column, which includes post-buckling deformations. Their results indicate consistent and symmetric hysteresis responses of this new concentric brace under cyclic loading. These studies have also proven far more energy dissipation capacity than the conventional concentric bracing system.

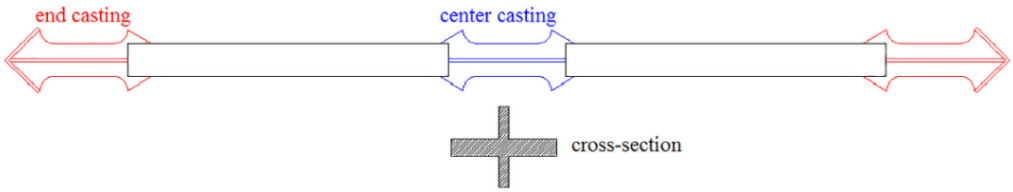

Figure 2. Schematic of the CMDB system.

The use of two-level or multi-level control systems is another method for improving the seismic behavior of structures, which has recently been under the focus of researchers. The main idea in these structural systems [10–14] is to combine different control systems with various stiffness and strength values, which results in desirable energy absorption in the structure for various earthquake intensities. Zahrai and Vosooq [11] introduced a dual system in which a combination of a vertical link beam and knee elements was used to maintain energy absorption. To improve the seismic performance in this structural system (Fig. 3a), the vertical link beam is used as an energy absorption element in the small loads area and knee elements are used for energy absorption under intense earthquakes. In another study, researchers introduced full steel double-stage yield buckling-restrained braces (DYB) (Fig. 3b) [13, 14]. The core plate of DYB consists of two small and big plates joined together serially. The deformation capacity of the small core is restricted by a stopper mechanism. At first, the deformation of DYB is focused on the small core and, when the stopper mechanism stops the deformation of this core, the displacement of DYB is transferred to the big core, hence DYBs have two stages of yielding. An experimental study conducted by Sun et al. showed that the DYB possesses higher energy dissipation capacity and seismic resistance than the traditional concentric bracing [13].

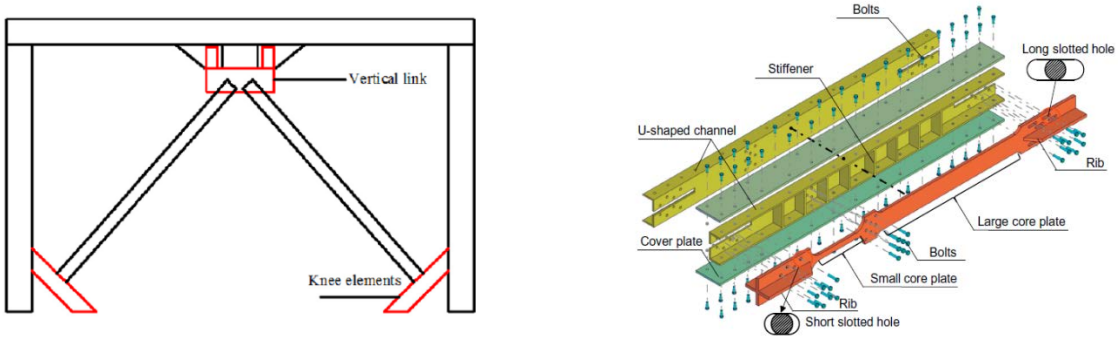

(a) Zahrai and Vosooq model **(b) DYB model**

Figure 3. Some kinds of two-level control systems.

Another invented structural system for improving seismic performance of structures with concentric bracings is the application of the buckling restrained brace (BRB) [15–19]. As shown in Fig. 4, this structural system uses bracings, including a casing and core, which removes the main shortcoming of the concentrically braced structural systems, i.e. buckling in compression [15, 16, 18]. Naghavi et al. [20] compared the response of BRB frames with the traditional concentrically braced ones. They found that the BRB system remarkably increased the ductility capacity and energy dissipation compared to the traditional concentrically braced frame. Qiu et al. [21] provided a method to correct the defect of the BRB system, that is, inability in reducing the residual drift story of the concentrically braced frames after an earthquake. In this study, the use of smart materials was suggested to remove the entire drift of residual story or make it negligible.

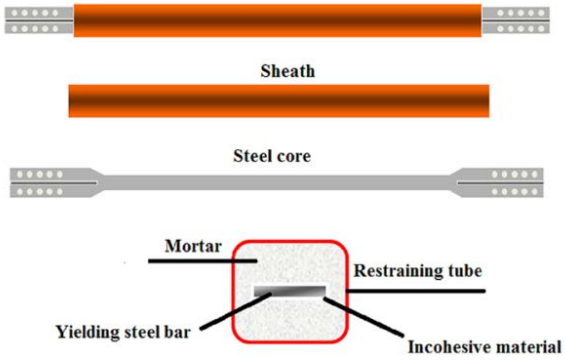

Figure 4. Buckling restrained brace (BRB) component.

Another method that has been developed as a substitute for conventional concentric braces is all-steel tube-in-tube buckling controlled brace, called (TinT-BCB) (Fig. 5) [22–24]. Seker and Shen [23] reported that the hysteresis response of this brace was consistent and symmetrical under cyclic loading. Factors affecting the response of these braces include the friction between tubes, the distance between the internal and external tubes, and the thickness ratio of the inner and outer tubes. In this brace, optimal performance generally results from a system with smallest possible gap, low friction, and a heavier outer tube.

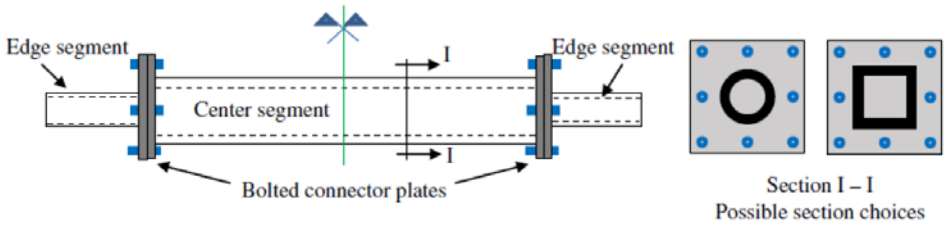

Figure 5. Seker et al. model [23].

Kachooee et al. [25] sought to reduce the input demand to the bracing joints by recommending a cross-section reduction fuse. According to Fig. 6, the fuse was placed within a particular length at the end of the brace. The results of this numerical study showed that the fuse not only reduced the input demand to the brace joints, but also the energy dissipation capacity of the bracing system. The reason was that reducing the cross-sectional area of the brace decreased the buckling capacity of the system, preventing the brace under cyclic loading from creating complete hysteresis loops and leading to a reduction in the energy dissipation capacity of the bracing system. In another study, Kafi and Kachooee tried to correct this defect using auxiliary elements placed around the fuse, resulting in the innovation of local fuse – auxiliary element concentric braces (LF-AECBs) (Fig. 7) [26].

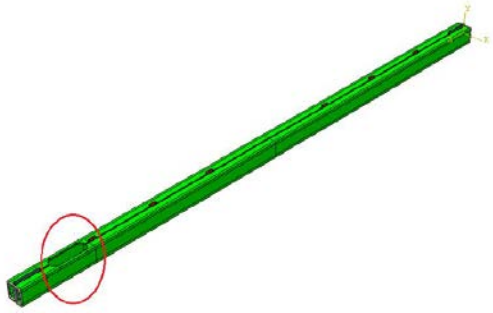

Figure 6. Kachooee et al. model.

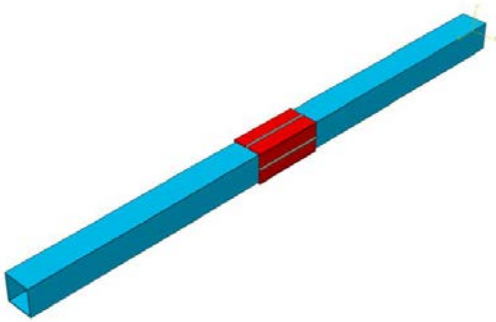

Figure 7. The LF-AECB model.

The results of this numerical study showed better performance of the new system in terms of energy dissipation and ductility capacity than that provided in [25]. However, the earlier buckling prevented the fuse capacity from being used thoroughly.

A new method is offered in this study to solve the problem of the fuse provided by Kafi and Kachooee [26] and improve the behavior of the concentric braces using numerical and experimental studies. In fact, the proposed formulation of LF-AECB bracing allows the coaxial bracing to exploit the fuse capacity until the failure. This increases the ductility and energy absorption of the proposed model. In this method, a local fuse is used along the brace with a newer formulation than that of Ref. [26]. The design of this local fuse is in such a way that the brace buckles locally and in the fuse length. In order to prevent fuse local buckling, auxiliary elements are used in the fuse region. This causes a symmetrical and stable behavior of the brace under cyclic loading, which results in optimal ductility and a considerable amount of energy dissipation capacity. A complete introduction of the mentioned brace, called improved LF-AECB (ILF-AECB), is provided in the following. Numerical studies were also done to determine its optimal shape in order to obtain maximum energy dissipation capacity and ductility in an ILF-AECB under cyclic loading. In the end, the responses of ductility, loadbearing capacity, and energy dissipation capacity of the concentrically braced frame equipped with the system suggested in this study are compared with a traditional similar concentrically braced frame using a numerical study conducted in ABAQUS 6.12 [27].

2. Methods

2.1. ILF-AECB bracing components

2.1.1. Formulation for calculating fuse area and length

The general pattern of the fuse (Fig. 8 and 9) for two different section-shapes of the brace indicates that the local fuse is generated by reducing the cross-section of the brace. Also, a transition zone has been considered to prevent stress concentration. Fig. 8 has shown two methods for creating the fuse in the box sections. In Fig. 8a, the sides of the fuse have been cut in the outer part to create the fuse. Also, in Fig. 8b, the method of creating the fuse has been presented through the internal cutting of box sides. It is worth mentioning that in Fig. 9, the method of creating the fuse for the braces with I section has shown, which have been reinforced with the vertical plates parallel to the web section. In this brace, the reinforcement plates have been removed in that area to create the fuse, and the cross-section of the brace has been decreased through this method.

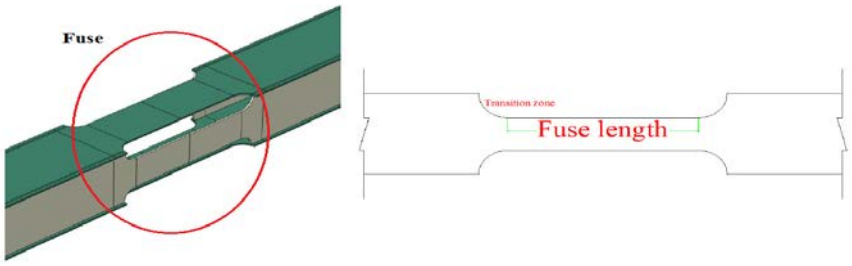

(a) creating the fuse through trimming external faces of the brace section

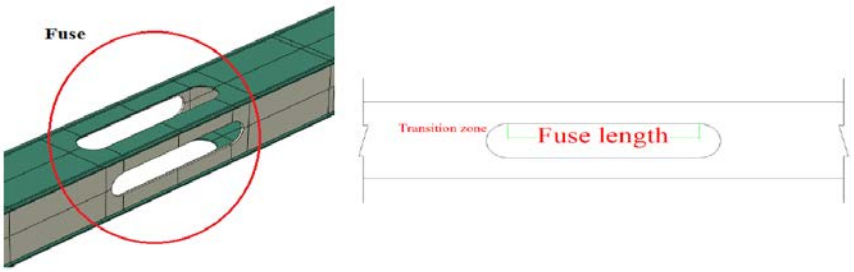

(b) creating the fuse through trimming internal faces of the brace section

Figure 8. Local fuse in the box-shape ILF-AECBs.

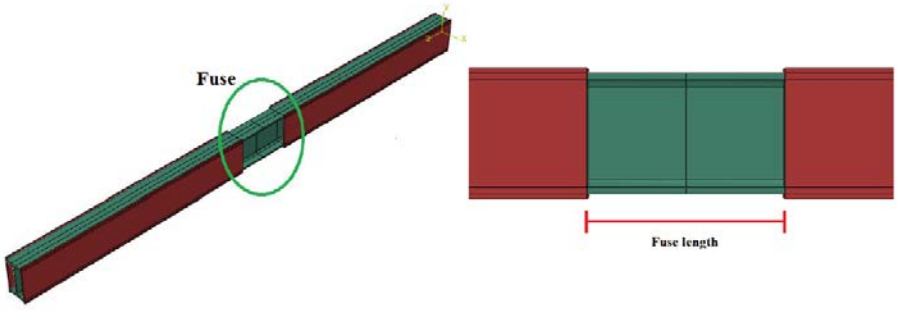

Figure 9. Local fuse in the I-shape ILF-AECBs.

In order to calculate the cross-sectional area of the fuse, the demand load exerted to the brace (P_{demand}) should first be obtained from the analyses. After calculating P_{demand}, Eq. (1) must be satisfied based on the Iranian steel structure code [28]:

$$P_{demand} \le 0.9P_{y,brace}, \tag{1}$$

where $P_{y,brace}$ is the yield load-bearing capacity of the brace and a coefficient of 0.9 is the strength reduction factor according to the Iranian steel structure code [28]. $P_{y,brace}$ can be calculated using Eq. (2):

$$P_{y,brace} = A_{brace} \cdot F_y, \tag{2}$$

where A_{brace} and F_y are the cross-sectional area and the yield stress of the brace materials, respectively. The cross-sectional area of the brace can be obtained using Eqs. (1) and (2):

$$A_{brace} \ge \frac{P_{demand}}{0.9F_y}. \tag{3}$$

After calculating the cross-sectional area of the brace, the slenderness coefficient of it should be checked to select the brace profile. The following expression should be controlled to make sure that the buckling of the brace does not take place before its yielding:

$$\left(\lambda_{brace} = \frac{k.l_{brace}}{r_{\min,brace}}\right) \le 80, \tag{4}$$

Ошибка! Закладка не определена.)

where λ_{brace}, k, l_{brace}, and $r_{\min,brace}$ are the slenderness factor, effective length coefficient, and the length of the brace and radius of gyration around the weak axis of the brace section, respectively. This must be examined to make sure that the buckling of the brace occurs after its yielding. In other words, this equation makes the designer choose a profile that satisfies it. The coefficient 80 is selected in accordance with ST37 steel materials according to DIN 17100, and if the material is changed, the desired value should be calculated according to the new material. The cross-sectional area of the fuse can be obtained after the verification of Eq. (4). For this purpose, the ultimate loadbearing capacity of the fuse, $P_{u,fuse}$ (Eq. (5)) can

be obtained from multiplying the steel material yield stress F_y by C_{pr} (the coefficient of material hardening) and R_y (the coefficient for the specifications of the brace profile) coefficients based on the Iranian steel structures code [28], which must be less than or equal to the minimum yield capacity of the brace, $P_{y,brace}$:

$$P_{u,\,fuse} = A_{fuse} \cdot R_y \cdot C_{pr} \cdot F_y \le \left(P_{y,brace} = A_{brace} \cdot F_y\right), \tag{5}$$

where A_{fuse} is the cross-sectional area of the fuse and R_y and C_{pr} can be obtained from Table 1 and Eq. (6) based on the Iranian steel structures code [28]:

Table 1. R_y coefficients for different shape sections of braces.

Section Shapes	R_y
Rolled tabular and box shape sections	1.25
Others rolled shape sections	1.2
Brace sections made of plates and belts	1.15

$$1.1 \le C_{pr} = \frac{F_y + F_u}{2F_u} \le 1.2. \tag{6}$$

In Eq. (6), F_u is final stress of the brace materials. According to Eq. (5), the cross-sectional area of the fuse can be calculated by Eq. (7):

$$A_{fuse} \le \frac{A_{brace}}{C_{pr} \cdot R_y}. \tag{7}$$

After calculating the cross-sectional area of the fuse, it must be verified whether or not the profile chosen for the fuse can tolerate the demand load. In other words, the fuse section is the critical unit of the brace that should tolerate the demand load exerted to the brace. Therefore, Eq. (8) should be modified as:

$$P_{demand} \le A_{fuse} \cdot F_y. \tag{8}$$

If Eq. (8) is satisfied, the selected profile is proper for both the fuse and the brace; otherwise, a new and bigger profile should be chosen and the calculations should be restarted. Based on the formulation obtained from Eq. (7) for calculating the cross-sectional area of the fuse, a numerical study is conducted using ABAQUS 6.12. The aim of this study is to examine the presented formulation and performance of the suggested method designed based on the mentioned formulation. In this study, a local fuse is calculated by Eq. (7) and placed in a distance of 25 cm from the end of a double-UNP120 brace. The length of the brace and fuse are respectively 414 cm and 5 cm. In order to prevent the local buckling of the fuse, the boxes have been installed as the auxiliary element and around the fuse with a 1-millimeter distance according to Fig. 10. Also, a stopper has been used in order to the concurrent horizontal movement of the internal and external auxiliary elements. This stopper has been tied to the external auxiliary element. The more detailed explanations about applying the auxiliary elements in ILF-AECB braces have been proposed in the 2.1.2 section of the paper. The mechanical specifications of the steel materials and the geometric specifications of the model are provided in Table 2. Also, the fixed end supports have been used in the study. In addition, the numerical model designed in ABAQUS 6.12 is illustrated in Fig. 10.

Table 2. Material mechanical properties and geometric properties of the studied model.

Yield stress	Ultimate stress	Yield strain	Ultimate strain	Area brace section	Area fuse section
2400 kg/cm^2	3700 kg/cm^2	0.0012	0.20	34 cm^2	22.60 cm^2

(a) general view of the model **(b) fuse position**

(c) auxiliary element details **(d) connection of inner box and stopper**

Figure 10. The numerical model in this study.

As shown in Fig. 11, the overall buckling takes place before the fuse reaches its ultimate loadbearing capacity. In other words, the hardening of steel material has caused the brace to reach its yield load before the fuse reaches the ultimate loadbearing capacity. According to Eq. (9), global buckling takes place in the model during the compressive cycle corresponding to the tensile cycle of the brace yielding due to a significant reduction in the stiffness compared to its elastic stiffness after yielding the materials.

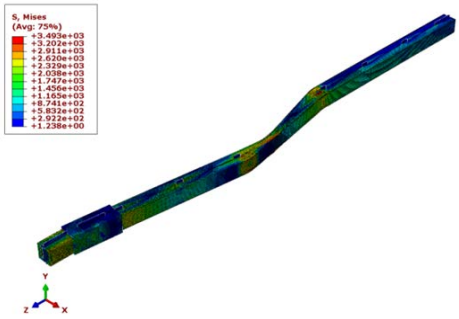

(a) global buckling of the brace before the fuse reaches its final load bearing capacity(Kg/cm^2)

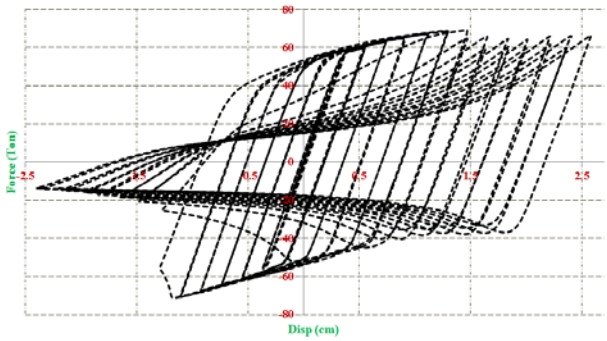

(b) hysteresis curve of the numerical model in this study

Figure 11. Results of the numerical study.

$$\sigma_{Cr} = \frac{\pi^2 \cdot E}{\lambda^2}. \quad (9)$$

In the above equation, σ_{Cr} is the critical stress, E is the elastic modulus, and λ is the slenderness factor of the element under compression.

According to the results obtained in this numerical study and using experimental results in real situations provided in a previous study by Bazzaz et al. [3–6], the steel yields a load less than the theoretical yield load. Therefore, a reduction coefficient of 0.8 is used in calculating yield capacity of the brace to make sure that the fuse reaches its ultimate loadbearing capacity and fails before the overall buckling of the brace. The studies provided in the following sections have confirmed that this value is suitable for the reduction coefficient. In addition, according to the experimental studies provided in this article, the ultimate stress of the steel materials, F_u, can be used directly instead of using $R_y \cdot C_{pr} \cdot F_y$ equation in the calculations of ultimate loadbearing capacity of the brace, which is provided by the Iranian steel structures code [28]. According to Table 3, the two experimental studies carried out here on braces with a box profile

made of plate and the braces with the I-beam profile have shown slight differences between the equation provided in the Iranian steel structures code [28] and the ultimate stress of the steel materials.

Table 3. Final stress values in comparison with those of $C_{pr} \cdot R_y \cdot F_y$ in the models.

Model name	$C_{pr} \cdot R_y \cdot F_y$ (MPa)	F_u (MPa)
Box shape brace	1.15·1.15·294=388.8	385
I shape brace	1.2·1.2·322=463.6	462.1

According to the above descriptions, Eqs. 5 and 7 are finally defined as the following, respectively:

$$P_{u,\,fuse} \le 0.8\left(P_{y,brace} = A_{brace} \cdot F_y\right); \tag{10}$$

$$A_{fuse} \le \frac{0.8.A_{brace} \cdot F_y}{F_u}. \tag{11}$$

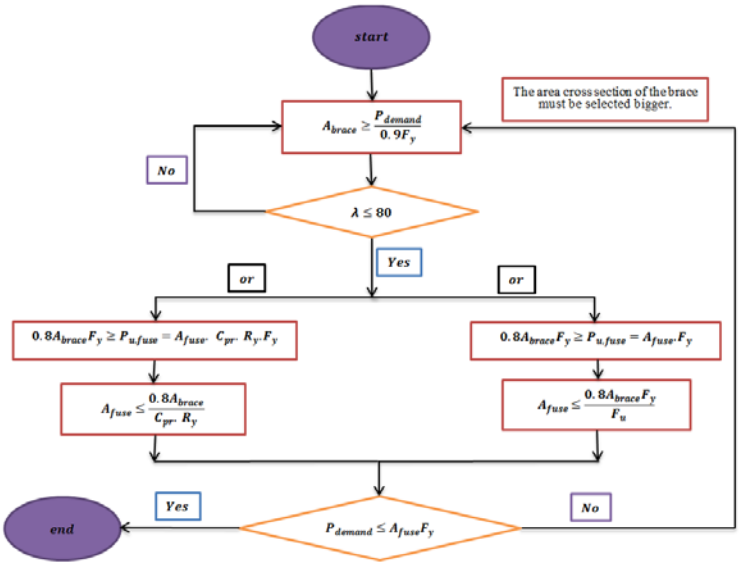

Figure 12. Flowchart of the brace and the fuse area calculation.

It should be noted that the capacity of the designed brace is equal to the fuse capacity based on Eq. (11), and the loadbearing capacity of the total cross-sectional area of the brace does not affect its loadbearing capacity. Moreover, the fuse length for ILF-AECBs is calculated in such a way that the fuse slenderness should be larger than the slenderness of the brace so that the overall buckling does not take place in the brace during the performance of the ILF-AECB against the exerted load. Due to this matter, Eq. (12) must be satisfied for ILF-AECBs:

$$l_{fuse} \ge \frac{k \cdot l_{brace}}{r_{min,brace}} \cdot r_{min,\,fuse}, \tag{12}$$

where $r_{min,brace}$ is the radius of gyration of the weakest piece of the fuse. Also, k is the compressive effective length coefficient of the element, which is chosen according to the end conditions of the brace.

2.1.2. Auxiliary elements in the ILF-AECB bracing

The second component in ILF-AECBs is the auxiliary element. Depend on the braces shape, auxiliary element can have several parts. For braces with a box-shape profile section, the auxiliary elements generally include the external and internal parts of the fuse with 1 mm distance from the fuse walls so that they cannot affect the fuse loadbearing capacity. The rationale behind the existence of the auxiliary element in the ILF-AECB is to prevent local buckling of the brace in the fuse area. As it is evident from Fig. 13, auxiliary element is made up of an inner rectangular tube and four outer channels for bracings with a box section.

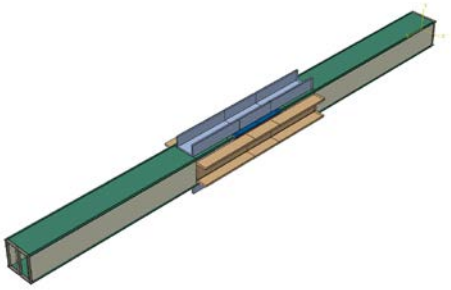

(a) general view of the brace equipped with ILF-AECB fuse

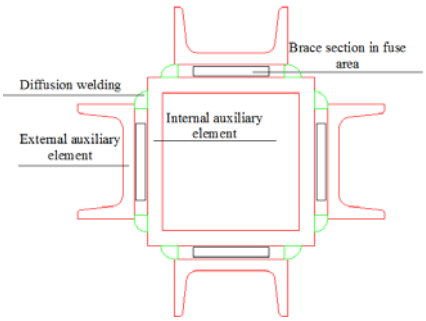

(b) section of the brace in fuse region

Figure 13. A box-shaped brace equipped with the ILF-AECB fuse.

The length of these internal and external elements should be at least 150 mm more than the fuse length plus the transition zones. The thickness of these elements must also be selected in such a way to be able to neutralize the lateral displacement of the fuse. To fix the position of the four external channels, one end of them must also be welded to the brace and to the inner tube throughout both sides of the channels in the fuse region using the diffusion welding (Fig. 13b), which also fixes the position of the inner tube.

In the I-shaped cross-section ILF-AECBs (Fig. 14), the auxiliary elements are composed of two steel elements placed within the web of the beam and reinforcing plates connected thereto. These elements are designed and placed in a manner to have a 1-mm gap between the web and reinforcing plates. As in the previous model, the length of the auxiliary elements must be at least 150 mm larger than all fuse ends, so that it has the necessary performance to prevent the fuse from local buckling. As shown in Fig. 14a, a stopper is used in the middle of the fuse length to fix the position of the auxiliary elements. According to this figure, stiffeners with a minimum thickness of 8 mm and a minimum width of 50 mm with a height equal to that of the reinforcing plate are also used to increase the strength of the reinforcing plates and prevent their local buckling in the fuse zone. These stiffeners must be placed on reinforcing plates approximately 50 mm apart from the edge of the plate and each other.

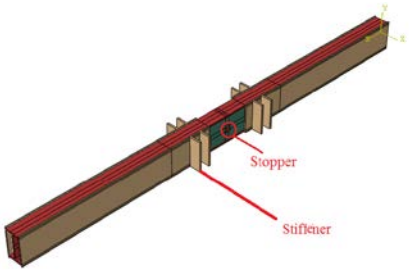

(a) general view of a brace equipped with ILF-AECB fuse

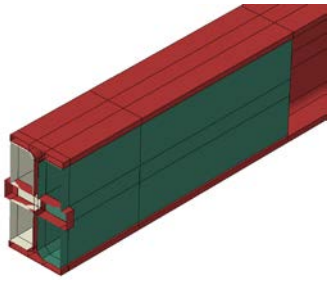

(b) section of a brace in fuse region

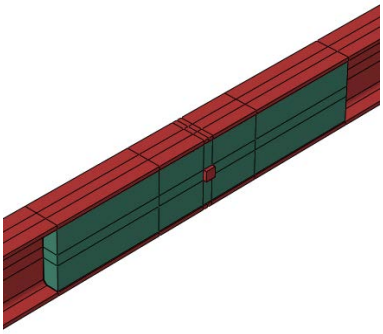

(c) auxiliary element position

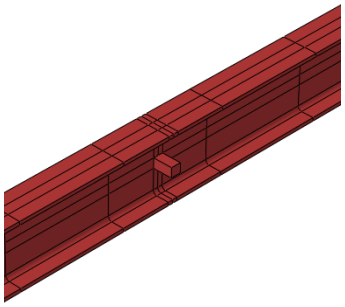

(d) the view of stopper

Figure 14. An I-shaped brace equipped with the ILF-AECB fuse.

It is noteworthy that in all the studies carried out for this paper, the used auxiliary elements surrounding fuse were so rigid and solid, thus the behavior of the studied braces was completely dependent on fuse behavior and no unusual behavior was seen in models due to auxiliary element weakness. However, it should be mentioned that inappropriate selection of surrounding auxiliary elements of the fuse in terms of rigidity and strength can surely affect the performance and proper behavior of ILF-AECBs. Thus,

it seems necessary to carry out an accurate study on the determination of rigidity and strength parameters for surrounding auxiliary elements of the fuse in the future.

3. Result and Discussion

3.1. Experimental study

3.1.1. Test setup, material properties, and loading pattern

In this study, an experimental research was conducted to investigate the behavior of the ILF-AECB bracing system. The studied brace models and their test setup are shown in Fig. 15. The brace sections are box-shaped and I-shaped in the first (Fig. 15a) and the second (Fig. 15b) models, respectively. The fully detailed of these shape sections has been presented in Fig. 16. According to Fig. 15, both ends of the models are welded to the end plates as fixed. The end plates are also connected to a rigid frame on one side using high resistance 10.9 bolts and a 100-ton load cell on the other side. A 200-ton jack was used to apply load to the models. According to Fig. 15, two strain gauges were also inserted in the middle distance between the end load plate and the center brace for both the models. Six and five LVDTs were also used in different parts of the models according to Fig. 15 (a and b).

(a) ILF-AECB brace with box-shaped section

(b) ILF-AECB brace with I-shaped section and reinforcement plates

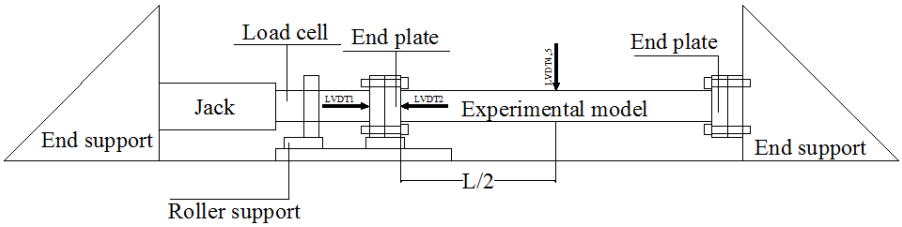

(c) Schematic diagram of the experimental specimens

Figure 15. Experimental setup.

The brace profile and the details of the fuse used for both the models are presented in Fig. 16. The length of all specimens is equal to 200 cm. The cross-sectional area and length of the fuse in the box-shape brace are considered equal to 792 mm^2 and 200 mm, respectively, based on Eqs. (2) and (3). These parameters in the I-shaped brace are 1320 mm^2 and 200 mm, respectively. For box-shape model

(Fig. 13b), a 100.100.6 mm box is the inner auxiliary element and four standard 60 mm channels are the external auxiliary elements. A length of 600 mm was selected for all auxiliary elements in both models.

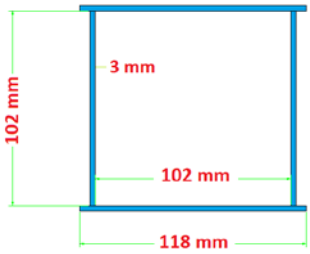

(a) cross-section of the box-shaped brace (mm)

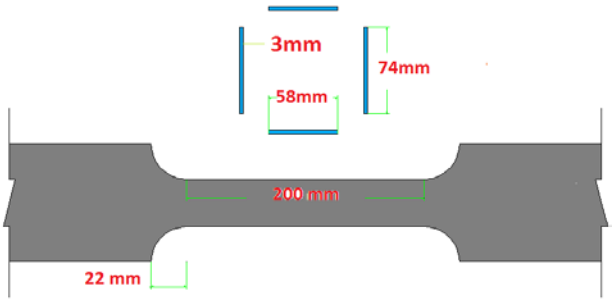

(b) fuse detail in the box-shaped brace (mm)

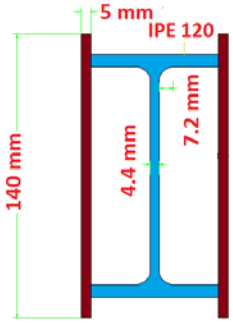

(c) cross-section of the I-shaped brace (mm)

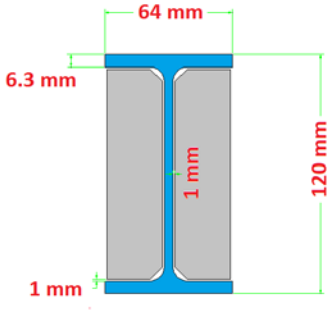

(d) fuse detail in the I-shaped brace (mm)

Figure 16. Details of the brace section and fuse in specimen models.

The steel materials(that were be ST37) used in the specimen models have specific mechanical characteristics (Table 4) that are obtained using the standard tensile test shown in Fig. 17. In this paper, the ATC-24 loading pattern [29] is used to obtain hysteresis responses of the experimental (section 3.1) and numerical (section 3.2) models, as shown in Fig. 18.

Table 4. Material properties.

Model		Yielding stress [MPa]	Yielding strain	Ultimate stress	Ultimate strain
Box-shape model		294	0.0025	385 MPa	0.1571
I-shape model	IPE12	308	0.0019	475 MPa	0.19
	Plate	265	0.0017	416 MPa	0.31

Figure 17. Standard tension test of steel material (based on the ASTM E8 standard).

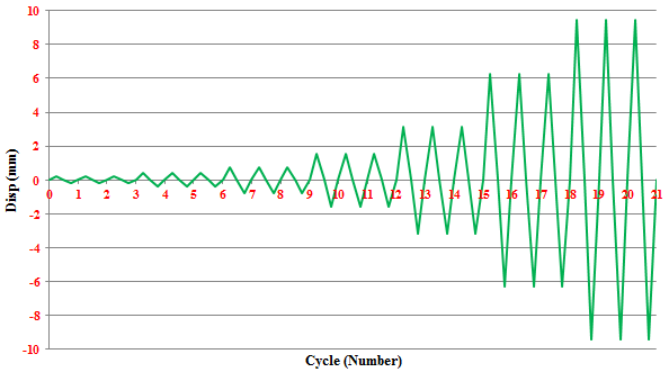

(a) Load pattern for the box-shaped model

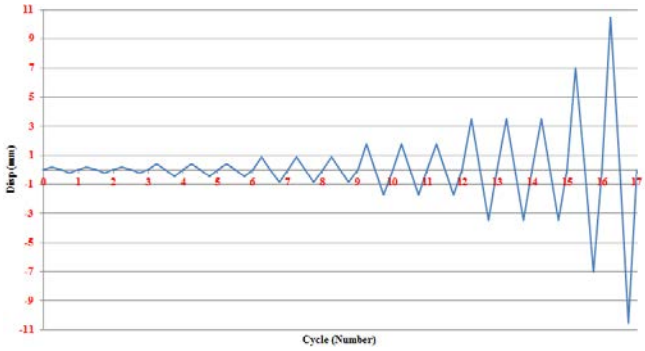

(b) Load pattern for the I-shaped model

Figure 18. The ATC24 load pattern.

3.1.2. Interpretation of experimental results

Fig. 19 represents the hysteresis curves obtained from the specimen models. As shown in this figure, the ILF-AECB has been able to provide a consistent and symmetric behavior under cyclic loading in these models. The tubby- and spindle-shaped curves obtained for the studied specimen models indicate that the mechanism defined in the ILF-AECB bracing system has been able to function correctly and prevent brace buckling. As shown in Fig. 19, the specimen models show no losses of the tensile and compressive strengths under cyclic loading. Besides, the corresponding load bearing capacity has also increased in the models with increasing the amount of displacement applied to the brace. The behavior of the box-shaped specimen model under cyclic loading is illustrated in Fig. 20. As shown in Fig. 20a, the internal and external auxiliary elements have succeeded in preventing the fuse from local buckling, so that the brace can continue to operate without the loss of strength in compressive load. According to Fig. 20b, the brace stops functioning and rupture occurs in the end zone of the fuse in the tensile loading cycle. The behavior of the I-shaped cross-section ILF-AECB bracing system is presented in Fig. 21. In this model, the auxiliary elements have also been able to prevent the fuse from the local buckling and eventually the brace is torn in the middle of the fuse in the tensile loading cycle (Fig. 21b). However, it is important to mention that the friction between the fuse components and auxiliary elements definitely resulted in the earlier failure of the fuse. This subject has decreased the fuse capacity in bearing of more deformation and energy absorption. The study of this topic, in detail, is necessary in the future.

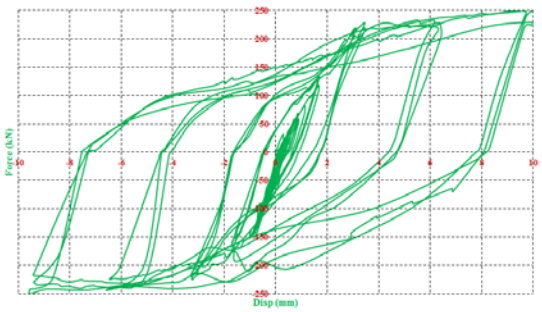

(a) Box-shaped ILF-AECB brace

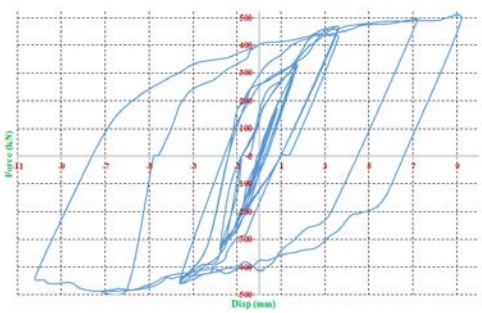

(b) I-shaped ILF-AECB brace

Figure 19. Hysteresis curve of specimen models.

(a) prevention of fuse local buckling by auxiliary elements

(b) tearing of brace at the end of the fuse

Figure 20. Failure of the box-shaped model.

The envelope curves of specimen models are presented in Fig. 22. According to these curves, the box-shaped model in the tensile region has undergone an initial yielding in the fuse region at a displacement of 0.3 mm and a corresponding load of 32.6 kN. In addition, the maximum load bearing capacity of the model (251.2 kN) occurred at a corresponding displacement of 10.2 mm; after this displacement, the model was raptured and broken in the fuse end zone. The brace offers a good performance in both the compressive and the tensile zones. In this zone, the braces have undergone an initial yielding at a displacement of 0.33 mm and a corresponding compressive load of 99.6 kN. Then, the brace was able to reach a maximum compressive load of 250.1 kN, which corresponds to a displacement of 9.54 mm. In the other model (Fig. 22b) the I-shaped cross-section ILF-AECB was able to provide a good performance in tensile and compressive loads. In the tensile region of this model, it has undergone an initial yield at a load of 97.5 kN and a displacement of 0.865 mm, and has experienced a maximum tensile strength of 493 kN at a corresponding displacement of 9.2 mm. In the compression zone, the mentioned specimen model withstands the compressive load without any buckling. In this region, an I-sectional specimen model has undergone an initial yield in a load of 209 KN and a corresponding displacement of 0.845 mm. Then, it was able to reach a maximum load bearing capacity of 487 kN at 7.2 mm displacement. The model has experienced a 438 kN load at a displacement of 10.2 mm in the compression zone during the last loading cycle. Finally, the model is torn in the center of the fuse after the last loading cycle and during the tensile loading cycle (Fig. 21b).

(a) prevention of the fuse local buckling by auxiliary elements

(b) tearing of the brace in the middle of the fuse

Figure 21. Failure of the I-shaped model.

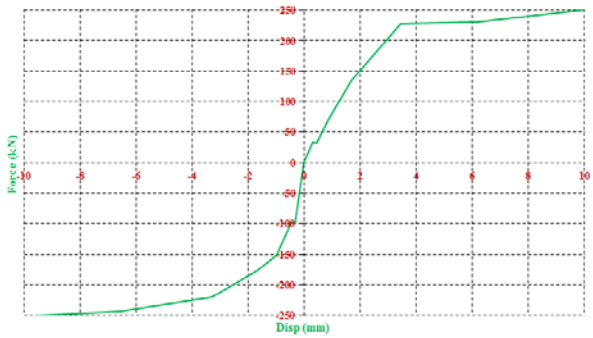

(a) Box-shaped ILF-AECB

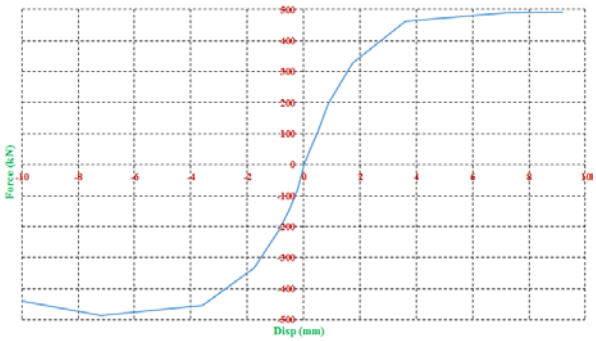

(b) I-shaped ILF-AECB

Figure 22. Envelope curves of specimen models.

With respect to the abovementioned issues and according to Eq. (13), the tensile ductility, μt, and the compressive ductility, μc, are 34 and 29 for the box-shaped specimen model, and 10.6 and 12 for the I-shaped specimen model, respectively. This amount of ductility, especially in the compression zone, is far greater than that of conventional concentric bracing systems, which indicates a more ductile behavior of the ILF-AECBs than that of conventional concentric braces.

$$\mu = \frac{\delta_u}{\delta_y}. \tag{13}$$

In Eq. (13), μ, δ_y, and δ_u, are the ductility, the yield displacement, and the ultimate displacement of the element, respectively.

The amounts of energy dissipated by the box-shaped and I-shaped specimen models were equal to 19728 kN.mm and 22283 kN.mm, respectively. Fig. 23 depicts the relative energy curves, ER, of the mentioned models. Each point in this curve represents the amount of energy dissipated by the brace in each loading cycle to the mean of the maximum compressive and tensile displacements corresponding to that cycle.

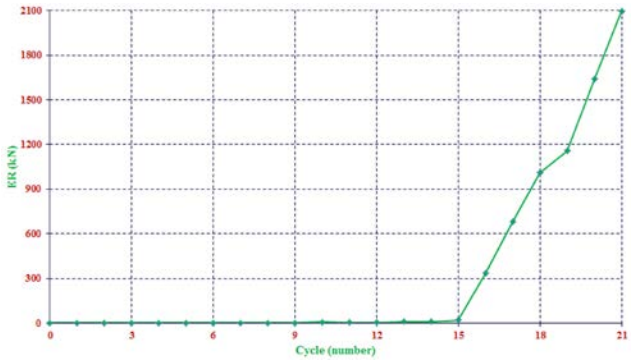

(a) Box-shaped ILF-AECB

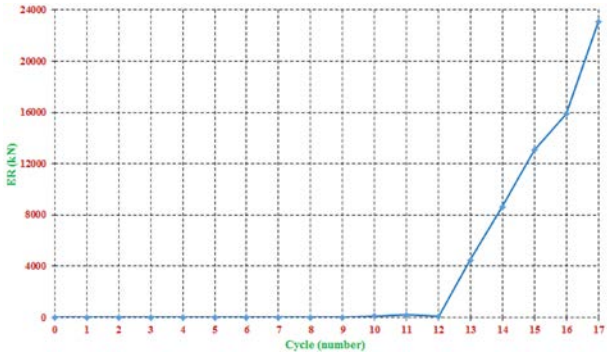

(b) I-shaped ILF-AECB

Figure 23. ER curves of specimen models.

Generally, when the amount of a brace energy dissipation increases with increasing the imposed displacement thereto, then it can be concluded that the brace has a desirable energy dissipation capacity, which is clearly shown in Fig. 23. With respect to this figure, it can be concluded that the ILF-AECBs are able to increase their relative energy dissipation capacity up to their ultimate performance due to the fact that buckling is not going to occur therein. In the case of common concentric bracing systems, however, the amount of ER decreases significantly after the overall buckling [26].

3.2. Numerical study

3.1.3. Verification of numerical study

First of all, the results of numerical studies need to be validated using the results of experimental studies. For this purpose, the Fuse-expr-box and Fuse-expr-I numerical models were generated corresponding to their specimen models in Abaqus 6.12 (2012) software using SOLID elements in three-dimensional form and then subjected to uniform loading (Fig. 13 and 14). The mechanical properties of the numerical models are provided in Table 4. These materials were defined in ABAQUS by a bi-linear curve with a moderate hardening slope in the plastic region (nearly 0.001 of elastic slope). This curve is symmetric

in tension and compression. In addition, the element contacts of the numerical models were defined by the Interaction Module and surface-to-surface contact. The tangential behavior of the contact areas in the numerical models was frictionless. To create buckling conditions for the entire numerical models, an initial displacement 0.01 times as large as the bracing length was applied to the middle of the bracing. The mesh size of 1 cm was applied. To more critical areas and the joints of two parts, a mesh size of 0.5 cm was applied. Also, C3D8I elements were applied to the meshing of all parts. The envelope curves of the specimen models and the capacity curves of numerical models are compared in Fig. 24. As shown in this figure, the numerical models have been able to provide a good estimate of the capacity of the specimen models.

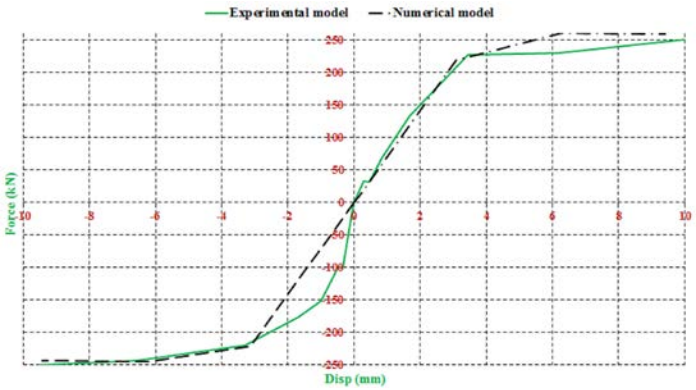

a) The box-shaped ILF-AECB

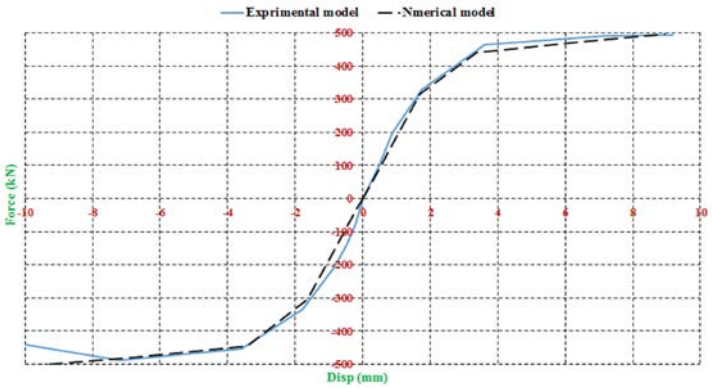

b) The I-shaped ILF-AECB

Figure 24. A comparison between envelope curves of specimen models and their corresponding numerical models.

3.1.4. The effect of the local fuse shape

This section examines the effect of the fuse shape on the box-shaped ILF-AECB hysteresis response. For this purpose, four models were made in the Abaqus 6.12 software (Fig. 25,). The Fuse-expr-box model corresponds to the specimen model, where the fuse is created by equally reducing the cross-sectional area on four sides of the brace section. In this model, the fuse is also created by trimming the outer region of the brace sides. In the Fuse-expr-2face model, the fuse is only created on two sides of the brace by trimming the outer zone of them. In the Fuse-cutside and Fuse-cutside-2face models, the fuses are also created by cutting the inner zone of the bracing sides, with the difference that the fuse is distributed equally on four sides of the brace in the former, but it is only created on two sides of the brace in the latter.

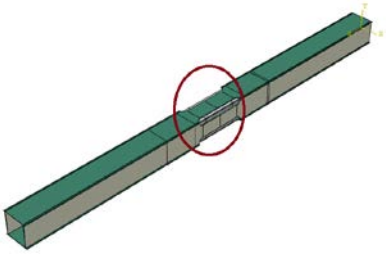

a) Fuse-expr-box model

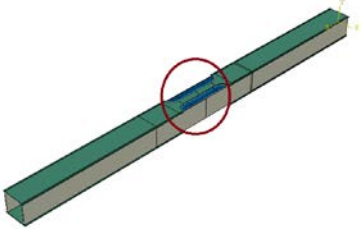

b) Fuse-expr-2face model

c) Fuse-cutside model **d) Fuse-cutside-2face model**

Figure 25. Numerical models for examining the influence of the fuse shape.

Fig. 26 compares the hysteresis responses of numerical models. As shown in this figure, the Fuse-cutside and Fuse-expr-box models, with fuses evenly distributed over their sides, have the most stable and tubby hysteresis curves. The Fuse-cutside model also offers better performance within the two models.

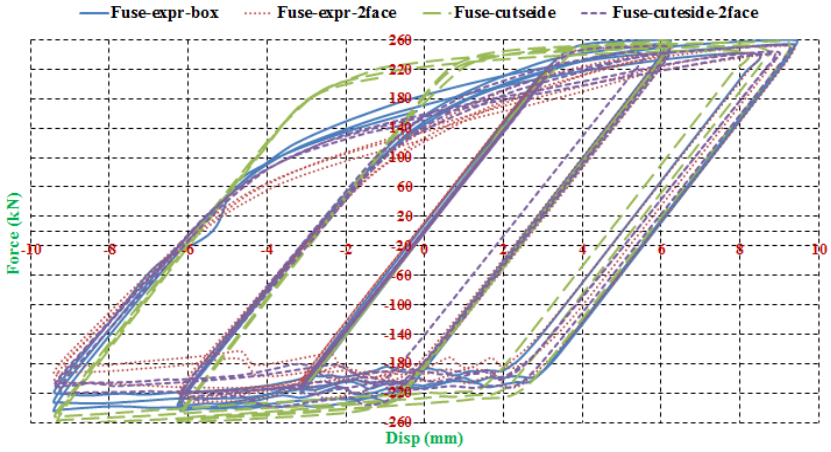

Figure 26. A comparison between hysteresis curves of box-shaped numerical models.

The overall behavior of numerical models is the same under cyclic loading, but minor differences in load bearing and energy absorption capacities have caused a distinction between them. The Fuse-expr-box model has the greatest maximum tensile load bearing capacity (260 kN). The maximum load bearing capacities are 258 and 252 kN in the Fuse-cutside model and in the other two models, respectively. The greatest maximum bearing capacity value among the studied numerical models is only about 3 % higher than the smallest values of these parameters. The Fuse-cutside model has maximum compressive load bearing capacity (262.5 kN), with values of 243, 232, and 238 kN in the Fuse-expr-box, Fuse-expr-2face, and Fuse-cutside-2face models, respectively. The maximum load bearing capacity of the Fuse-cutside model was 8 %, 13 %, and 10 % higher than the Fuse-expr-box, Fuse-expr-2face, and Fuse-cutside-2face, respectively. Also, the energy dissipated by the Fuse-cutside model (21411 kNmm) is higher than those of 19728, 17474, and 18492 kNmm for Fuse-expr-box, Fuse-expr-2face, and Fuse-cutside-2face models, respectively. In other words, the Fuse-cutside model has been able to dissipate about 8.5 %, 22.5 %, and 16 % more energy than Fuse-expr-box, Fuse-expr-2face, and Fuse-cutside-2face models, respectively, under the cyclic loading. According to the content presented in this section, it can be concluded that the ILF-AECB provides its best performance against cyclic loading, when the localized fuse is evenly distributed between the bracing faces and is created by trimming its internal zone of those faces.

In the case of I-shaped cross-section ILF-AECB, the most optimal and economical form of the brace cross section is the same as what presented for the Fuse-expr-I model. As seen in the box cross-section ILF-AECB, the maximum difference in the energy dissipation capacity was 22.5 % between the compared models. However, if it is required to form a new shape of the fuse in I-shaped cross-section braces, it will require a local cut in I section part of the brace and the reinforcing plates connected thereto. This fact will greatly increase the cost of constructing I-shaped cross-section ILF-AECBs, making them uneconomical. However, in the ILF-AECBs with I cross-section, which is similar to the Fuse-expr-I model, the fuse can easily be implemented at no cost in the construction site. Therefore, it can be concluded that even an improvement of 22.5 % in the energy dissipation capacity, which is the maximum improvement of this parameter, is not considered a significant improvement in comparison to the increase in the implementation cost of the I-shaped cross-section ILF-AECB in fuse shapes, except for the fuse shape in the Fuse-expr-I model. For this reason, the study on the various fuse shapes in I-shaped section braces is ignored herein.

3.3. Comparative analysis study

In this section of the study, the behavior of ILF-AECB frames is compared with that of the conventional concentrically braced frame. For this purpose, a 5-story building with a chevron braced lateral resistant system was first designed with the assumption of symmetry and regularity in the plan and height based on the Iranian steel structures code [28] using the ETABS 9.7.4 software [30]. The plan of the building is illustrated in Fig. 27. The height of all stories and the width of all spans are 3 m 4 m, respectively. According to these dimensions, the frame diagonal, which is equal to the length of the brace, is 3.61 m. The building frame was designed with the assumption that the frame to the ground, the beam to the column, and the brace to the frame are all connected in a pinned manner. Furthermore, the building location was assumed to be in Tehran city and the type of the soil was assumed to be D in the analysis. The dead and live loads of the stories were respectively assumed to be 540 and 200 kg/m^2, while those of the roof were assumed to be 570 and 150 kg/m^2, respectively. In addition, the load of the walls was distributed uniformly and was considered to be 195 kg/m^2.

After the completion of the analysis, the maximum force in the braces of each story was extracted from the ETABS software. Then, the brace was designed based on the formulation of the ILF-AECB. The profiles of the fuse and the brace, as well as the fuse length were obtained based on Eqs. 11 and 12, respectively. In order to classify the profiles of the building, the design forces for the braces of the first and second floors were considered the same as the maximum force (41 ton) of the first floor. For other floors, the maximum force of the brace was the same as that (25 ton) in the third floor. Interestingly, the smallest choice profile of the brace should be Box120*120*8 in designing the braces to satisfy Eq. (4), with assumptions of yield stress and ultimate stress being equal to 2400 and 3700 kg/cm^2, respectively (the slenderness of the brace is less than 80).

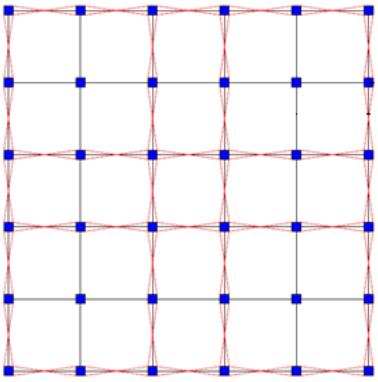

Figure 27. The plan of the studied analytical model.

The cross-sectional area of this profile is 35.84 cm^2 and that of the fuse is 20.8 cm^2 for the mentioned profile based on Eq. (11). Hence, the designed fuse in this profile has a yield load of 51 ton. In other words, the smallest selected profile of the brace, which is obtained based on the slenderness equation, automatically satisfies both demand loads. Due to the points mentioned above, therefore, the bracing profile in all spans and floors was considered to be Box120*120*8. Also, the fuse length is 25 cm for the profile mentioned above based on Eq. (12). After obtaining the profile for the brace, the beams and columns for the building mentioned above with the chevron bracing resistant system were designed using ETABS. The final structural elements obtained from the design are provided in Table 5.

Table 5. Structural elements of the studied models.

Story	Brace	Beam	Column	Fuse Area (cm^2)	Fuse Length (cm)
1	BOX120*120*8	IPE160	BOX160*160*12.5	20.80	25
2	BOX120*120*8	IPE160	BOX160*160*10	20.80	25
3	BOX120*120*8	IPE160	BOX120*120*10	20.80	25
4	BOX120*120*8	IPE160	BOX120*120*10	20.80	25
5	BOX120*120*8	IPE160	BOX120*120*10	20.80	25

After the above steps and designing the building, a frame of the building was extracted (all braced frames of the building were the same) to compare the behavior of the ILF-AECB frame with that of the conventional concentrically braced frame. Then, this frame was modeled in ABAQUS with two different modes as a 2D model. In the first mode, the frame was modeled as a concentrically braced frame, named CBF, in ABAQUS software (Fig. 28). In the second mode, a model was created named the ILF-AECB,

where the beams and columns are the same as the previous model (CBF), but the brace is modeled as ILF-AECB. In this model, the brace is divided into three parts. At the two ends, the profile of Box120*120*8, which was obtained from the design and used for the CBF model, is used for this case. In the middle, which is 30 cm away from the end of the brace with a length equal to the fuse length (25 cm), an element is embedded with the same cross-sectional area of the fuse (20.8 cm^2). For modeling the auxiliary elements to prevent the fuse from local buckling, this section of the brace was restricted locally with defining a specific boundary condition, which avoids the displacement of the fuse in the direction perpendicular to the length of the brace. Fig. 29 shows the ILF-AECB model. A 2D beam element with shear flexible linear meshing was used in all the modeling processes.

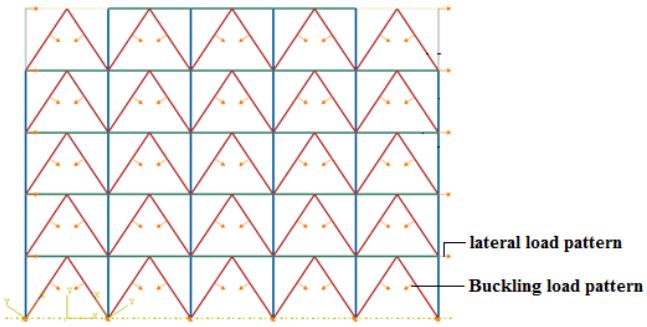

Figure 28. The CBF model.

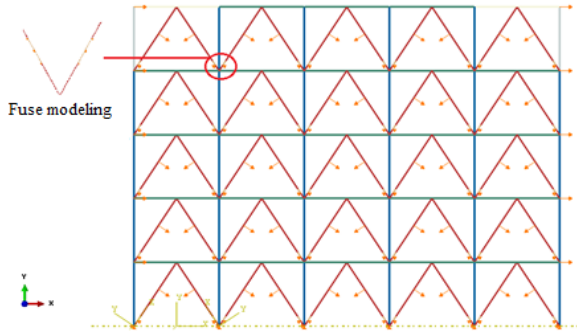

Figure 29. The ILF-AECB model.

After the completion of modeling, a nonlinear static analysis was done for each model to compare the response of the ILF-AECB with that of the CBF. An inverted triangle displacement loading plan with a displacement pitch of 2 mm was used in both analyses. After analyzing the models, the curves of their capacities were obtained as shown in Fig. 30, showing that the base shear of the ILF-AECB model is less than that of the CBF model for all displacement pitches. The maximum difference of the base shear between both models is 15 % in the elastic area, which varies from 15 % to 20 % in the non-elastic area with increasing the displacement. This shows that the use of ILF-AECBs in the structure reduces the base shear, which is the base of designing the main structural elements in comparison to the conventional concentrically braced frame, resulting in the use of lighter structural elements in the structure and thus reducing the construction costs of the structure. Moreover, the lower base shear in the ILF-AECB than that of the CBF model demonstrates that the fuse elements in the former have desirably lessened the input energy to the structure, which is also proved previously in the numerical and experimental studies.

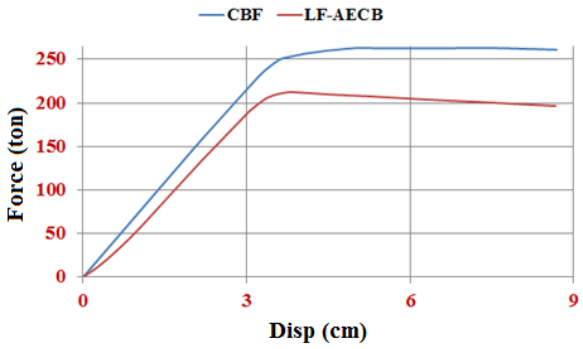

Figure 30. Comparing the capacity curves of analytical models.

In order to compare the lost energy by the ILF-AECB frame with that of the concentrically braced frame, two one-story single-span frames of the first story of the above mentioned frames were chosen (Fig. 31) and underwent a displacement nonlinear static cyclic loading. After modeling the frames, a displacement loading pattern with a displacement step of 2 mm was applied to the columns of the frames in a cyclic form (Fig. 31). Then, the hysteresis curves of the frames were obtained as in Fig. 32.

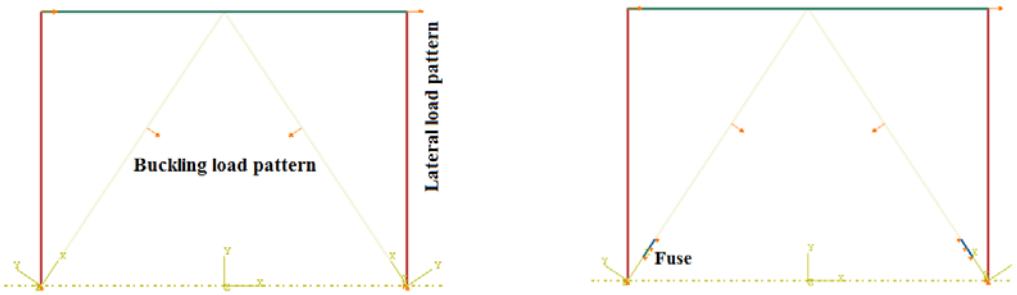

CBF model **ILF-AECB model**

Figure 31. One-story one-opening studied frames.

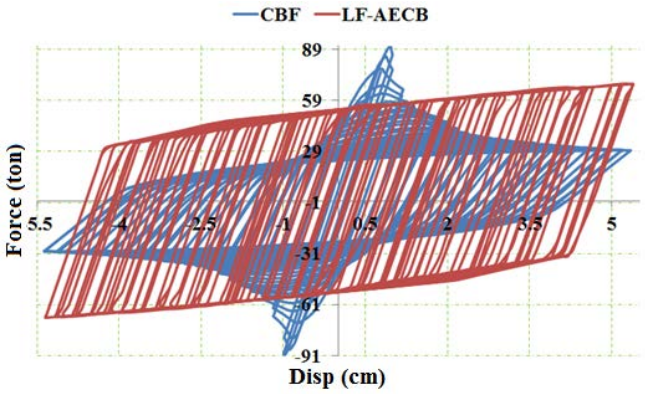

Figure 32. Hysteresis curves of studied frames.

As shown in Fig. 32, the conventional concentrically braced frame had a significant initial elastic stiffness as expected, and it could withstand a base shear of 91 ton elastically without any energy absorption. After this load and due to the buckling of the braces, the frame lost its loadbearing capacity, and its load decreased from 91 ton to about 29 ton (almost 69 % reduction). The energy absorption of this frame was around 121.5 ton·m. However, the scenario is different in the ILF-AECB frame, which entered the non-linear area from a base shear of 50 ton and began to absorb the energy due to the existence of the locally restricted fuses in this frame. Afterward, the frame could tolerate loads up to 68.5 ton of the base shear in larger loading cycles due to the hardening of the steel materials of the fuse without any sudden drop in the loadbearing capacity. The dissipated energy in this frame was about 243.5 ton·m. According to the above points, it is finally concluded that the ILF-AECB could provide more stable behavior, more energy absorption (about two times), and lower maximum base shear (about 15%) than the CBF frame. This would be expected from the ILF-AECB frame before performing the nonlinear static analysis. The final deformation of the frame is illustrated in Fig. 33.

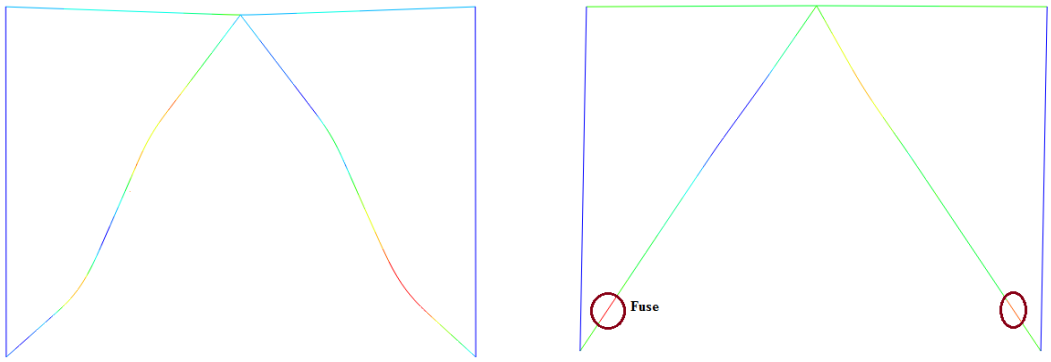

Brace buckling in the CBF model **Inelastic deformation concentration in the fuse location in the ILF-AECB model**

Figure 33. Final deformations(cm) in the studied frames.

4. Conclusion

In this study, a new ILF-AECB has been introduced as an alternative to conventional concentric bracings using numerical and experimental studies. The rationale behind the creation of the ILF-AECB is to improve the behavior of this element in the compressive zone by preventing the concentric brace from buckling. For this reason, a local fuse was created in the brace to prevent the overall buckling in the brace and the bracing buckling was limited locally to this zone. Then, the local buckling was prevented through the use of auxiliary elements in the fuse region, which resulted in a stable and symmetric cyclic response, and thus, tubby and spindle shaped hysteresis curves were created for this element under cyclic loading. Therefore, the following results are presented in this study:

- The ILF-AECB provides a stable and symmetric response to cyclic loading because it uses a restricted lateral fuse mounted on the ILF-AECB, which prevents it from buckling and causes the brace to have a desirable performance in a compressive zone as the tensile zone.
- Due to the absence of brace buckling, the ILF-AECB has a very high ductility in the compressive zone, as the tensile zone, while conventional concentric braces have an undesirable ductility due to the brace buckling in the compressive zone, and in many cases, the bracing behavior is considered only in the tensile region.
- The ER curve is ascending for the ILF-AECB, meaning that the energy dissipated in each cycle of displacement loading increases significantly with displacement increment in the brace. In conventional concentric braces, however, the amount of ER reduces significantly after brace buckling and, as a result, full brace capacity will not be used for energy dissipation.
- The shape of the local fuse applied to the brace is an effective factor in the box-shaped ILF-AECB system cyclic response. According to the results of this article, it can be concluded that the optimal fuse shape for getting the best performance of the box-shaped ILF-AECB system will be achieved when the fuse is evenly distributed between the brace sides and is obtained by trimming the internal regions of these faces, as in the Fuse-cutside model. In the case of I-shaped cross-section ILF-AECBs, the energy absorption improvement is not very significant as to become superior to economical aspect of its construction because the optimal economical form of the fuse type is the same as that used in the Fuse-expr-I model and in the other modes of the fuse shape. Therefore, the other fuse shapes were ignored in these bracings.
- In this article, a comparison of the analytical studies between the single-span one-story frame of the LF-AECB and the conventional single-span one-story concentrically braced frame showed more stable performance, lower base shear (about 15 %), and more energy dissipation (about two times) for the LF-AECB frame.

References

1. Moghaddam, H., Estekanchi, H. On the characteristics of off-centre bracing system. Journal of Constructional Steel Research. 1995. 35 (3). Pp. 361–376. DOI: 10.1016/0143-974X(94)00050-R
2. Moghaddam, H., Estekanchi, H. Seismic behavior of off-centre bracing systems. Journal of Constructional Steel Research. 1999. 51 (2). Pp. 177–196. DOI: 10.1016/S0143-974X(99)00007-3
3. Bazzaz, M., Kheyroddin, A., Kafi, M.A., Andalib, Z. Evaluation of the seismic performance of off-centre bracing system with ductile element in steel frames. Steel and Composite Structures. 2012. 12(5). Pp. 445–464. DOI: 10.12989/scs.2012.12.5.445
4. Bazzaz, M., Kheyroddin, A., Kafi, M.A., Andalib, Z., Esmaeili, H. Evaluating the seismic performance of off-centre bracing system with circular element in optimum place. International Journal of Steel Structures. 2014. 14 (2). Pp. 293–304. DOI: 10.1007/s13296-014-2009-x
5. Bazzaz, M., Andalib, Z., Kafi, M.A., Kheyroddin, A. Evaluating the performance of OBS-C-O in steel frames under monotonic load. Earthquakes and Structures. 2015. 8 (3). Pp. 697–710. DOI: 10.12989/eas.2015.8.3.699
6. Bazzaz, M., Andalib, Z., Kheyroddin, A., Kafi, M.A. Numerical comparison of the seismic performance of steel rings in off-centre bracing system steel rings in off-centre bracing system. Steel and Composite Structures. 2015. 19 (4). Pp. 917–937. DOI: 10.12989/scs.2015.19.4.917
7. Federico, G., Fleischman, R., Ward, K. Buckling control of cast modular ductile bracing system for seismic-resistant steel frames. Journal of Constructional Steel Research. 2012. 71. Pp. 74–82. DOI: 10.1016/j.jcsr.2011.11.010
8. Ward, K.M., Fleischman, R.B., Federico, G. A cast modular bracing system for steel special concentrically braced frames. Engineering Structures. 2012. 45. Pp. 104–116. DOI: 10.1016/j.engstruct.2012.05.025
9. Seker, O., Akbas, B., Seker, P.T., Faytarouni, M., Shen, J. Three-segment steel brace for seismic design of concentrically braced frames. Journal of Constructional Steel Research. 2017. 137. Pp. 211–227. DOI: 10.1016/j.jcsr.2017.06.035
10. Balendra, T., Yu, C.H., Lee, F.L. An economical structural system for wind and earthquake loads. Engineering Structures. 2001. 23. Pp. 491–501. DOI: 10.1016/S0141-0296(00)00061-4
11. Zahrai, S.M., Vosooq, A.K. Study of an innovative two-stage control system: Chevron knee bracing & shear panel in series connection. Structural Engineering and Mechanics. 2013. 47 (6). Pp. 881–898. DOI: 10.12989/sem.2013.47.6.881
12. Cheraghi, A., Zahrai, S.M. Innovative multi-level control with concentric pipes along brace to reduce seismic response of steel frames. Journal of Constructional Steel Research. 2016. 127. Pp. 120–135. DOI: 10.1016/j.jcsr.2016.07.024

13. Jiangbo, S., Peng, P., Haishen,W. Development and experimental validation of an assembled steel double-stage yield buckling restrained brace. Journal of Constructional Steel Research. 2018. 145. Pp. 330–340. DOI: 10.1016/j.jcsr.2018.03.003
14. Barbagallo, F., Bosco, M., Marino, E.M., Rossi, P.P. Achieving a more effective concentric braced frame by the double-stage yield BRB. Engineering Structures. 2019. 186. Pp. 484–497. DOI: 10.1016/j.engstruct.2019.02.028
15. Iwata, M., Kato, T., Wada, A. Buckling-restrained braces as hysteretic dampers. 3rd International Conference STESSA. 2000. Montreal. Canada.
16. Sabelli, R., Mahin, S., Chang, C. Seismic demands on steel braced frame buildings with buckling-restrained braces. Engineering Structures. 2003. 25 (5). Pp. 655–66. DOI: 10.1016/S0141-0296(02)00175-X
17. Kiggins, S., Uang, C.M. Reducing residual drift of buckling-restrained braced frames as a dual system. Engineering Structures. 2006. 28 (11). Pp. 1525–1532. DOI: 10.1016/j.engstruct.2005.10.023.
18. Hoveidae, N., Tremblay, R., Rafezy, B., Davaran, A. Numerical investigation of seismic behavior of short-core all-steel buckling restrained braces. Journal of Constructional Steel Research. 2015. 114. Pp. 89–99. DOI: 10.1016/j.jcsr.2015.06.005
19. Maurya, A., Eatherton, M.R., Matsui, R., Florig, S.H. Experimental investigation of miniature buckling restrained braces for use as structural fuses. Journal of Constructional Steel Research. 2016. 127. Pp. 54–65. DOI: 10.1016/j.jcsr.2016.07.019
20. Naghavi, M., Rahnavard, R., Thomas, R.J., Malekinejad, M. Numerical evaluation of the hysteretic behavior of concentrically braced frames and buckling restrained brace frame systems. Journal of Building Engineering. 2019. 22. Pp. 415–428. DOI: 10.1016/j.jobe.2018.12.023
21. Qiu, C., Zhang, Y., Li, H., Qu, B., Hou, H., Tian, L. Seismic performance of Concentrically Braced Frames with non-buckling braces: A comparative study. Engineering Structures. 2018. 154. Pp. 93–102. DOI: 10.1016/j.engstruct.2017.10.075
22. Shen, J., Seker, O., Sutchiewcharn, N., Akbas, B. Cyclic behavior of buckling-controlled braces. Journal of Constructional Steel Research. 2016. 121. Pp. 110–125. DOI: 10.1016/j.jcsr.2016.01.018
23. Seker, O., Shen, J. Developing an all-steel buckling controlled brace. Journal of Constructional Steel Research. 2017. 131. Pp. 94–109. 2017. DOI: 10.1016/j.jcsr.2017.01.006
24. Momenzadeh, S., Seker, O., Faytarouni, M., Shen, J. Seismic performance of all-steel buckling-controlled braces with various cross-sections. Journal of Constructional Steel Research. 2017. 139. Pp. 44–61. DOI: 10.1016/j.jcsr.2017.09.003
25. Kachooee, A., Kafi, M.A., Gerami, M. The Effect of Local Fuse on Behavior of Concentrically Brace Frame by a Numerical Study. Civil Engineering Journal. 2018. 4 (3). Pp. 655–667. DOI: 10.28991/cej-0309123
26. Kafi, M.A., Kachooee, A. The behavior of concentric brace with bounded fuse. Magazine of Civil Engineering. 2018. 78. Pp. 16–29. DOI: 10.18720/MCE.78.2
27. ABAQUS Ver .6.12. User's Manual. RI. USA. 2012.
28. Guidelines for design of steel structures .The tenth chapter of the National Building Regulations. Iran. 2013.
29. Zhou, F., Fang Ch., Chen, Y. Experimental and numerical studies on stainless steel tubular members under axial cyclic loading. Engineering Structures. 2018. 171. Pp. 72–85. DOI:10.1016/j.engstruct.2018.05.093
30. ETABS Ver 9.7.4. User's Manual. CSI. USA. 2005.

Information about author:

***Ali Kachooee**, PhD*
ORCID: https://orcid.org/0000-0003-3648-2905
E-mail: ali.kachooee@semnan.ac.ir

Received 10.10.2021. Approved after reviewing 21.06.2022. Accepted 22.06.2022.